

Holographic Phase Retrieval and Optimal Reference Design

David A. Barmherzig* Ju Sun† Emmanuel J. Candès‡ T.J. Lane§ Po-Nan Li¶

June 14, 2022

Abstract

A general mathematical framework and recovery algorithm is presented for the holographic phase retrieval problem. In this problem, which arises in holographic coherent diffraction imaging, a “reference” portion of the signal to be recovered via phase retrieval is a priori known from experimental design. A general formula is also derived for the expected recovery error when the measurement data is corrupted by Poisson shot noise. This facilitates an optimization perspective towards reference design and analysis. We employ this optimization perspective towards quantifying the performance of various reference choices.

1 Introduction

1.1 Phase Retrieval and Coherent Diffraction Imaging

The phase retrieval problem concerns recovering a signal from the squared magnitude of its Fourier transform. The problem can be stated symbolically as

$$\begin{array}{ll} \textbf{Given} & |\hat{X}(\omega)|^2 \doteq \left| \int_{t \in T} X(t) e^{-i\omega t} \right|^2 \quad \text{for } \omega \in \Omega, \\ \textbf{Recover} & X \end{array} \quad (1.1)$$

where T and Ω are the (possibly multidimensional) domains of the signal and its Fourier transform, respectively. Phase retrieval arises ubiquitously in scientific imaging, where one seeks to “image” or determine the structure of an object from various phaseless data measurements. Such settings include crystallography [1], diffraction imaging [2], optics [3], and astronomy [4].

Phase retrieval has gained enormous attention over the last two decades, largely due to an emerging imaging technique known as Coherent Diffraction Imaging, or CDI [5] (illustrated in Fig. 1). In CDI, a coherent beam source, often being an X-ray, is illuminated upon a sample of interest. Upon the beam reaching the sample, diffraction occurs and secondary electromagnetic waves are emitted which travel until reaching a far-field detector. The detector measures the photon flux and hence records the resulting diffraction pattern, which is approximately proportional to the squared magnitude of the Fourier transform of the electric field of the sample. The structure of the sample can then, in principle, be reconstructed from the diffraction pattern by solving the phase retrieval problem [6, 7, 8]. With the advent of extremely powerful X-ray light sources, such as X-ray Free-Electron Lasers (XFELs) [9] and synchrotron radiation [10], CDI is pushing the frontier of high-resolution imaging of biological and material specimens at the nanoscale [11, 12, 13, 14].

*Institute for Computational and Mathematical Engineering, Stanford University, Stanford, CA 94305, U.S.A.

†Department of Mathematics, Stanford University, Stanford, CA 94305, U.S.A.

‡Department of Mathematics and Department of Statistics, Stanford University, Stanford, CA 94305, U.S.A.

§SLAC National Accelerator Laboratory, Menlo Park, CA 94025, U.S.A.

¶Department of Electrical Engineering, Stanford University, Stanford, CA 94305, U.S.A.



Figure 1: CDI setup. Image courtesy of [15].

1.2 Phase Retrieval Algorithms

The solution to the phase retrieval problem is not unique, due to certain intrinsic ambiguities caused by the combination of Fourier transform and the quadratic measurement (more in Section 2.1). Also, modulo the unavoidable ambiguities, the solution is still not always unique: the problem is serious for one-dimensional signals, and much milder for two- or high-dimensional signals [16, 8, 17]. For CDI, the focus is on 2D or even 3D signals. When the solution is unique up to the intrinsic ambiguities, phase retrieval can be naturally posed as various forms of nonconvex optimization problems, which entail a formidable computational challenge—solving a nonconvex optimization problem is well known to be difficult [18].

In practice, alternating-projection type algorithms are commonly employed to solve the resulting nonconvex problems. The most notable and popular algorithm of this type is Fienup’s Hybrid Input-Output (HIO) algorithm [19]. Other practical variants based on the same alternating projection idea include Relaxed Averaged Alternating Reflections (RAAR) [20], Difference Map [21], and Alternating Direction Method of Multipliers (ADMM) [22, 23, 24]. While often successful, these algorithms have no theoretical guarantees. They are also known to suffer from various problems such as stagnation at erroneous solutions, slow runtime, sensitivity to noise and parameter tuning [25, 26].

To mitigate the above uniqueness and algorithmic issues, a line of recent work has proposed to modify the typical CDI setup. They sequentially modulate either the beam pattern or the Fourier transform via random or deterministic masks and hence gather multiple-shot measurements [27, 28, 15, 29, 30]. Several of these proposals have resulted in efficient algorithms with correctness guarantees [15, 31, 29]. However, such a multiple-shot experiment can inflict damage on certain fragile specimens [8].

1.3 Holographic CDI and Holographic Phase Retrieval

In this paper, we consider a different line of modifications to CDI based on the holography idea introduced by Gabor in 1948 [32], which we shall term as *holographic CDI*. In holographic CDI, the experiment remains single-shot, but a “reference” area, whose structure is a priori known, is included in the diffraction area alongside the sample of interest (see Fig. 2 for the system setup and Fig. 3 for a schematic illustration).

Introducing the reference substantially simplifies the resulting phase retrieval problem, which we call *holographic phase retrieval*: the computational problem is now a linear deconvolution, which is equivalent to solving a linear system [35, 36, 37, 38]. The entailing computation can be further streamlined when certain specific reference shapes are employed. Due to the simplicity and power, holographic CDI is growing in its impact and popularity [39, 33].

In the imaging community, popular reference choices are the pinhole reference [40], the slit reference [37, 41, 42], and the block reference [43, 44, 38], as illustrated in Fig. 4. Other proposed references include L-shapes [37], parallelograms [37], and annuluses [39]. These reference shapes are typically realized as “empty space” cut out from a surrounding metal apparatus (see, e.g., Fig. 2). To solve the resulting holographic phase retrieval problem, often only reference-specific recovery procedures are provided, e.g., the recent

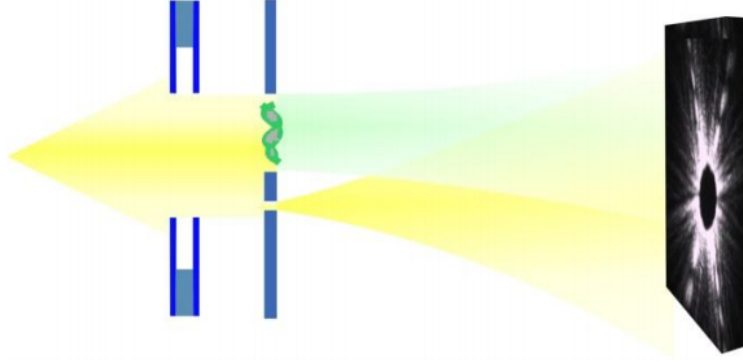


Figure 2: Holographic CDI setup. Image courtesy of [33].

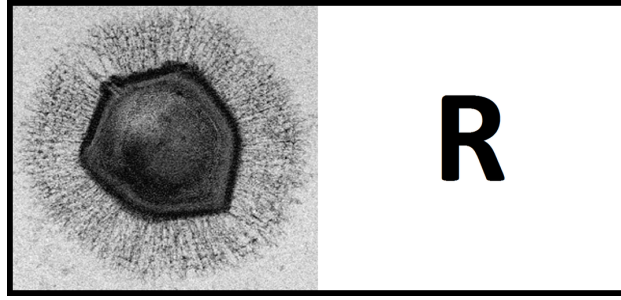


Figure 3: The diffraction area in Holographic CDI contains an unknown specimen (here shown as a mimivirus [34]) together with a known reference (here shown as “R”). Popular choices for the reference R are shown in Fig. 4.

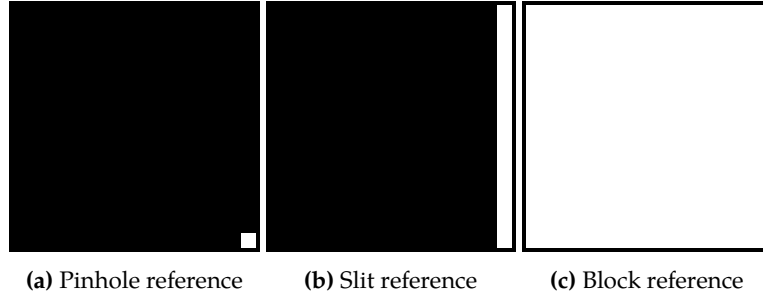


Figure 4: Schematic of the three leading reference choices for Holographic CDI. (Images have 16×16 enlarged pixels for illustration.)

deterministic recovery algorithm HERALDO [37, 41, 42] for a couple of well-structured references. Only recently has the underlying linear deconvolution idea been articulated more generally and formally [38, 45]. Moreover, studies of these methods have to date been almost entirely empirical. Some error analysis of the classical deconvolution method and HERALDO is provided in [46].

1.4 Our Contributions

In this paper, we derive a general computational and analysis framework for holographic phase retrieval.

- The framework allows for a detailed characterization of the deconvolution procedure in terms of solving

a structured linear system. We show how particular reference choices further simplify the linear system. This explains why fast, specialized algorithms (e.g., see [40, 43, 37]) can be designed for these reference choices. Our presentation also underscores that the deconvolution-based recovery algorithm—which we term *referenced deconvolution*—returns the least-squares solution to the noise-corrupted holographic phase retrieval problem.

- Based on the framework, we obtain a simple formula for the expected recovery error from noisy data. This error formula proves to be a useful tool for experimental design and simulation, and allows for viewing reference design from an optimization perspective. We further simplify the error formula for a practical Poisson shot noise model and thereby give novel characterizations of popular reference choices. For example, we show that the pinhole reference (Fig. 4a) is the unique reference choice which places equal weights on all frequencies contributing to the recovery error. In this sense, the pinhole frequency is an optimal design choice for “flat-spectrum” data. By contrast, the block reference (Fig. 4c) provides the minimum zero-frequency error contribution, and “near-minimal” error contributions for low frequencies.

Numerical results demonstrate the power of the proposed referenced deconvolution method and the optimality of the block reference for recovering typical imaging specimens. We also view this work as a means to introduce the holographic phase retrieval problem and the optimal reference design problem to a wider mathematical and scientific audience.

2 Holographic Phase Retrieval and Referenced Deconvolution

We set up the phase retrieval problem and basic notations in Section 2.1. Then, we present the holographic phase retrieval problem in Section 2.2 and our general algorithm, referenced deconvolution, in Section 2.3. We close this section by specializing our algorithm to three particular reference choices in Section 2.4.

2.1 The Phase Retrieval Problem

We consider the discrete two-dimensional phase retrieval problem. This setting is manifested in practical CDI experiments, since CCD detectors can only take measurements at a finite number of pixel locations.

For a signal $X \in \mathbb{C}^{n_1 \times n_2}$, let \hat{X} be the size $m_1 \times m_2$ discrete Fourier transform of X given by

$$\hat{X}(k_1, k_2) = \sum_{t_1=0}^{n_1-1} \sum_{t_2=0}^{n_2-1} X(t_1, t_2) e^{-2\pi i(t_1 k_1 / m_1 + t_2 k_2 / m_2)}, \quad k_1 \in \{0, \dots, m_1 - 1\}, k_2 \in \{0, \dots, m_2 - 1\}. \quad (2.1)$$

Whenever $m_1 \geq n_1$ and $m_2 \geq n_2$, the Fourier transform is injective and is said to be *oversampled*. The mapping can also be compactly expressed as matrix multiplication:

$$\hat{X} = F_L X F_R^T, \quad (2.2)$$

where $F_L \in \mathbb{C}^{m_1 \times n_1}$ and $F_R \in \mathbb{C}^{m_2 \times n_2}$ are the corresponding discrete Fourier transform (DFT) matrices given by

$$\begin{aligned} F_L(k, t) &= e^{-2\pi i k t / m_1} \quad \text{for } (k, t) \in \{0, \dots, m_1 - 1\} \times \{0, \dots, n_1 - 1\}, \\ F_R(k, t) &= e^{-2\pi i k t / m_2} \quad \text{for } (k, t) \in \{0, \dots, m_2 - 1\} \times \{0, \dots, n_2 - 1\}. \end{aligned}$$

When $m_1 \geq n_1$ and $m_2 \geq n_2$, both F_L and F_R have linearly independent columns which are orthogonal to each other, and so the inverse mapping is given simply by

$$X = \frac{1}{m_1 m_2} F_L^* \hat{X} (F_R^*)^T. \quad (2.3)$$

The forward and inverse transforms in Eqs. (2.2) and (2.3) can also conveniently be expressed as a single matrix multiplication based on matrix Kronecker products. Let $\text{vec}(\cdot)$ be the columnwise vectorization operator acting on matrices and \otimes denote the matrix Kronecker products. The following result can be directly verified:

Lemma 2.1. $Y = AXB \iff \text{vec}(Y) = (B^T \otimes A) \text{vec}(X)$.

Applying Lemma 2.1 to Eqs. (2.2) and (2.3) gives

$$\text{vec}(\hat{X}) = (F_R \otimes F_L) \text{vec}(X), \quad (2.4)$$

$$\text{vec}(X) = \frac{1}{m^2} (F_R^* \otimes F_L^*) \text{vec}(\hat{X}), \quad \text{when } m_1 \geq n_1 \text{ and } m_2 \geq n_2. \quad (2.5)$$

We are now ready to define the Fourier phase retrieval problem in two-dimensional, discrete setting.

Definition 2.2. The Fourier *phase retrieval* problem consists of recovering a signal $X \in \mathbb{C}^{n_1 \times n_2}$ given the squared magnitudes of its Fourier transform, i.e. all entries in $|\hat{X}|^2 \in \mathbb{C}^{m_1 \times m_2}$.

Here exact recovery is not possible, as the mapping $X \mapsto |\hat{X}|^2$ is not injective due to the following intrinsic ambiguities:

1. Global phase shift: if $X \mapsto |\hat{X}|^2$, $X e^{i\theta} \mapsto |\hat{X}|^2$ for any $\theta \in [0, 2\pi)$;
2. Conjugate-flipping: if $X \mapsto |\hat{X}|^2$, $Y \mapsto |\hat{X}|^2$ for $Y \in \mathbb{C}^{n_1 \times n_2}$ with $Y(t_1, t_2) = \overline{X(n_1 - 1 - t_1, n_2 - 1 - t_2)}$ for all t_1, t_2 .

Moreover, if X has zero boundary rows or columns, shifted copies of X whose nonzero rows and columns remain in range also produce the same set of measurements. In fact, all possible compositions of the three ambiguities lead to signals “physically equivalent” to X with exactly the same magnitude measurements $|\hat{X}|^2$. Thus, recovering X from $|\hat{X}|^2$ shall be understood as recovery up to these symmetries.

Definition 2.3. For signals $X, Y \in \mathbb{C}^{n_1 \times n_2}$ both indexed over $\{0, 1, \dots, n_1 - 1\} \times \{0, 1, \dots, n_2 - 1\}$, the cross-correlation $C_{[X,Y]} \in \mathbb{C}^{(2n_1-1) \times (2n_2-1)}$ between X and Y is defined as

$$C_{[X,Y]}(s_1, s_2) = \sum_{t_1=0}^{n_1-1} \sum_{t_2=0}^{n_2-1} X(t_1, t_2) \overline{Y(t_1 - s_1, t_2 - s_2)}, \quad (2.6)$$

for $(s_1, s_2) \in \{-(n_1 - 1), \dots, n_1 - 1\} \times \{-(n_2 - 1), \dots, n_2 - 1\}$, where any $X(t_1, t_2)$ or $Y(t_1 - s_1, t_2 - s_2)$ in the summands that is outside the valid index range is taken as 0.

When $X = Y$, this is known as the *autocorrelation* of X , and is denoted by A_X . Let \hat{X} be the size $m_1 \times m_2$ Fourier transform of X . It is well-known that [47]

$$|\hat{X}|^2 = \widehat{A_X}, \quad (2.7)$$

where

$$\begin{aligned} \widehat{A_X} &= F_{LA} A_X F_{RA}^T \quad \text{with } F_{LA} \in \mathbb{C}^{m_1 \times (2n_1-1)}, m_1 \geq 2n_1 - 1 \quad F_{RA} \in \mathbb{C}^{m_2 \times (2n_2-1)}, m_2 \geq 2n_2 - 1 \\ &\text{and } F_{LA}(k, t) = e^{-2\pi i k t / m_1} \forall (k, t) \in \{0, \dots, m_1 - 1\} \times \{-(n_1 - 1), \dots, n_1 - 1\}, \\ &\text{and } F_{RA}(k, t) = e^{-2\pi i k t / m_2} \forall (k, t) \in \{0, \dots, m_2 - 1\} \times \{-(n_2 - 1), \dots, n_2 - 1\}. \end{aligned} \quad (2.8)$$

Moreover, as $m_1 \geq 2n_1 - 1$ and $m_2 \geq 2n_2 - 1$, the mapping $A_X \mapsto \widehat{A_X}$ is injective, and hence A_X can be recovered from $\widehat{A_X}$, or equivalently $|\hat{X}|^2$ by the corresponding inverse transform:

$$A_X = \frac{1}{m_1 m_2} F_{LA}^* |\hat{X}|^2 (F_{RA}^*)^T. \quad (2.9)$$

Since A_X is uniquely determined from the $m_1 \geq 2n_1 - 1, m_2 \geq 2n_2 - 1$ uniform frequency sampling points and A_X in turn uniquely determines the entire frequency spectrum (by taking the 2D discrete-time Fourier transform), any oversampling past the $m_1 = 2n_1 - 1, m_2 = 2n_2 - 1$ threshold provides no additional information.¹ This is in some sense the phase retrieval analogue of the Shannon sampling theorem [48].

A powerful result by Hayes [16] establishes that for all two- or higher-dimensional signals, excluding a set of Lebesgue measure zero, the only transformations on X which preserves $|\widehat{X}|^2$ are the aforementioned physically equivalent symmetries. Thus, phase retrieval is generically well-posed in two or higher dimensions.

2.2 Holographic Phase Retrieval and Deconvolution

For simplicity of exposition, henceforth we focus on square $X \in \mathbb{C}^{n \times n}$. Suppose a reference $R \in \mathbb{C}^{n \times n}$ of the same size is placed on the right next to X , i.e., as illustrated in Fig. 3. So now we have $[X, R] \in \mathbb{C}^{n \times 2n}$:

$$[X, R](t_1, t_2) = \begin{cases} X(t_1, t_2) & t_2 \in \{0, \dots, n-1\} \\ R(t_1, t_2) & t_2 \in \{n, \dots, 2n-1\}. \end{cases}$$

We may assume without loss of generality that the magnitudes of the entries of X and R are within the interval $[0, 1]$. This convention has the physical interpretation of indicating the (average) *transmission coefficient* of the specimen around each pixel location. Roughly speaking, transmission coefficient measures the fraction of incident electromagnetic radiation that is transmitted, rather than being reflected or absorbed and is a material property (e.g. see Fig. 5). For example, later on we are especially interested in reference setups that are shapes cut from a surrounding opaque apparatus: for the opaque part the transmission coefficient is 0, whereas for the cut-off part the coefficient is 1. Fig. 5 shows the typical transmission coefficient of polycarbonate at different photon energy levels.

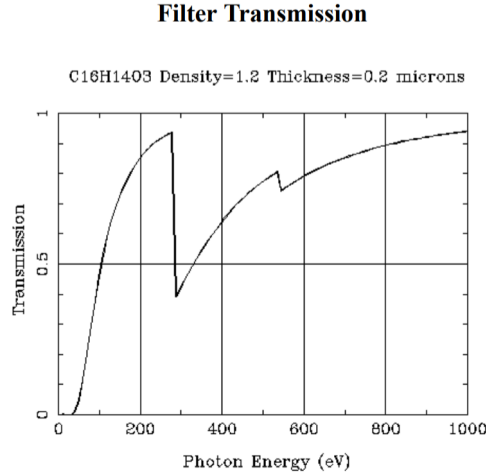


Figure 5: Average transmission coefficient of polycarbonate at different photon energies [49].

In the above setting, the *holographic phase retrieval* problem is:

Holographic phase retrieval: given $|\widehat{[X, R]}|^2 \in \mathbb{R}^{m_1 \times m_2}$, recover $X \in \mathbb{C}^{n \times n}$.

Again for simplicity, henceforth we assume $m_1 = m_2 = m$ with $m \geq 4n - 1$. We can then recover the autocorrelation of $[X, R]$, $A_{[X, R]}$, by taking the inverse Fourier transform on $|\widehat{[X, R]}|^2$. So under that oversampling assumption, we effectively have $A_{[X, R]}$. To see how the reference R helps to significantly simplify

¹This is true at least when there is no noise.

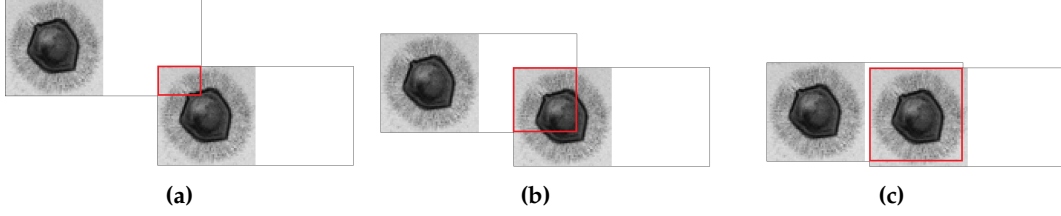


Figure 6: Near the boundary of the index range, each successive auto-correlation value of $[X, R]$ is formed by the overlap of a subregion of X with a subregion of R , which effectively gives a new linear measurement of X , as R is known. The original image can then be recovered via solving the linear system in Eq. (2.12) with enough such linear measurements.

the subsequent retrieval problem, we can think over the autocorrelation process, referring to Fig. 6: in obtaining the autocorrelation sequence, we fix one copy of $[X, R]$, move around (in \mathbb{R}^2) another copy, and calculate and record the inner product of the overlapped region (if any) of the two copies each time. When the overlap covers only part of R in one copy and only part of X in the other, we are effectively taking a linear measurement of X . Since X contains only n^2 free variables, linear algebra tells that n^2 non-degenerate linear measurements provide sufficient information for recovering X —from Fig. 6, obviously this is possible and one can just take one contiguous quadrant of the cross-correlation between X and R , which is again one segment of $A_{[X,R]}$! The resulting problem is simply a linear deconvolution problem.

The exact correspondence is formalized as follows. For $(s_1, s_2) \in \{-(n-1), \dots, 0\} \times \{-(n-1), \dots, 0\}$,

$$\begin{aligned}
 C_{[X,R]}(s_1, s_2) &= \sum_{t_1=0}^{n-1} \sum_{t_2=0}^{n-1} X(t_1, t_2) \overline{R(t_1 - s_1, t_2 - s_2)} \\
 &= \sum_{t_1=0}^{n-1} \sum_{t_2=0}^{n-1} [X, R](t_1, t_2) \overline{[X, R](t_1 - s_1, t_2 + n - s_2)} \\
 &= \sum_{t_1=0}^{n-1} \sum_{t_2=0}^{2n-1} [X, R](t_1, t_2) \overline{[X, R](t_1 - s_1, t_2 + n - s_2)} \quad (\text{zero-filling rule in Definition 2.3}) \\
 &= A_{[X,R]}(s_1, -n + s_2).
 \end{aligned} \tag{2.10}$$

Since this is only a quadrant of the whole cross-correlation $C_{[X,R]}$, we shall write this part as $C_{[X,R]}^\diamond$. The above correspondence can be compactly written as

$$C_{[X,R]}^\diamond = P_1 A_{[X,R]} P_2^T, \tag{2.11}$$

where $P_1 = [I_n, 0_{n \times (n-1)}]$ and $P_2 = [I_n, 0_{n \times (3n-1)}]$.

For a fixed R , $C_{[X,R]}^\diamond$ is clearly linear in X . This linear relationship can be expressed conveniently as

$$\text{vec}(C_{[X,R]}^\diamond) = M_R \text{vec}(X), \tag{2.12}$$

for a corresponding matrix $M_R \in \mathbb{R}^{n^2 \times n^2}$, which can be constructed by inspection of Eq. (2.10). It is easy to verify that for any choice of R , M_R is lower-triangular and block-Toeplitz. We illustrate the form of M_R using a simple example. Suppose

$$R = \begin{bmatrix} r_{00} & r_{01} & r_{02} \\ r_{10} & r_{11} & r_{12} \\ r_{20} & r_{21} & r_{22} \end{bmatrix},$$

then

$$M_R = \begin{bmatrix} \overline{r_{22}} & 0 & 0 & 0 & 0 & 0 \\ \overline{r_{12}} & \overline{r_{22}} & 0 & 0 & 0 & 0 \\ \overline{r_{02}} & \overline{r_{12}} & \overline{r_{22}} & 0 & 0 & 0 \\ \hline \overline{r_{21}} & 0 & 0 & \overline{r_{22}} & 0 & 0 \\ \overline{r_{11}} & \overline{r_{21}} & 0 & \overline{r_{12}} & \overline{r_{22}} & 0 \\ \overline{r_{01}} & \overline{r_{11}} & \overline{r_{22}} & \overline{r_{02}} & \overline{r_{12}} & \overline{r_{22}} \\ \hline \overline{r_{20}} & 0 & 0 & \overline{r_{21}} & 0 & 0 \\ \overline{r_{10}} & \overline{r_{20}} & 0 & \overline{r_{11}} & \overline{r_{21}} & 0 \\ \overline{r_{00}} & \overline{r_{10}} & \overline{r_{20}} & \overline{r_{01}} & \overline{r_{11}} & \overline{r_{21}} \end{bmatrix}.$$

Note that M_R is invertible if and only if $R(n-1, n-1) \neq 0$. This invertibility condition is equivalent to the well-known “holographic separation condition” [37], dictating when an image is recoverable via a reference object. Geometrically, it guarantees that there is no aliasing corrupting the cross-correlation.

Provided that $m \geq 4n-1$ and $R(n-1, n-1) \neq 0$, we then have

$$\begin{aligned} \text{vec}(X) &= M_R^{-1} \text{vec}(C_{[X,R]}^\diamond) \\ &= M_R^{-1} \text{vec}(P_1 A_{[X,R]} P_2^T) \\ &= \frac{1}{m^2} M_R^{-1} \text{vec}(P_1 F_{LA}^* |\widehat{[X, R]}|^2 (F_{RA}^T)^* P_2^T), \end{aligned} \quad (2.13)$$

where $F_{LA} \in \mathbb{C}^{m \times (2n-1)}$ and $F_{RA} \in \mathbb{C}^{m \times (4n-1)}$ are centered DFT matrices, similar to that defined in Eq. (2.8).

Applying Lemma 2.1,

$$\text{vec}(X) = T_R \text{vec}(|\widehat{[X, R]}|^2), \quad (2.14)$$

where

$$T_R = \frac{1}{m^2} M_R^{-1} [(P_2 F_{RA}^*) \otimes (P_1 F_{LA}^*)]. \quad (2.15)$$

This gives a linear mapping between the squared Fourier transform magnitudes $|\widehat{[X, R]}|^2$ and the ground truth signal X .

2.3 Referenced Deconvolution

Combining Eqs. (2.13) and (2.14) gives an algorithm for recovering X given R and $Y \doteq |\widehat{[X, R]}|^2$. In practice, the measurements $|\widehat{[X, R]}|^2$ almost always contain noise, and we shall write the possibly noisy version as Y^* . The algorithm then produces a least-squares solution given the noisy measurement Y^* , as summarized below.

Theorem 2.4 (Referenced Deconvolution for Holographic Phase Retrieval). *Let $X \in \mathbb{C}^{n \times n}$ be an unknown signal, $R \in \mathbb{C}^{n \times n}$ a known “reference” signal with $R(n-1, n-1) \neq 0$, and $Y \doteq |\widehat{[X, R]}|^2$ size $m \times m$ Fourier transform of $[X, R]$ with $m \geq 4n-1$. Given Y^* , which is a possibly noisy version of Y , and the known reference R , the following algorithm yields the solution to the least-squares problem*

$$\min_{X \in \mathbb{C}^{n \times n}} \|Y^* - |\widehat{[X, R]}|^2\|^2 : \quad (2.16)$$

1. Given Y^* , apply an inverse Fourier transform ($\mathbb{C}^{m \times m} \mapsto \mathbb{C}^{(2n-1) \times (4n-1)}$) to obtain $A_{[X,R]}^*$, an estimate of the autocorrelation $A_{[X,R]}$;
2. Select the top-left $n \times n$ submatrix of $A_{[X,R]}^*$, denoted as $C_{[X,R]}^{\diamond*}$, which is an estimate of the top-left $n \times n$ quadrant of the cross-correlation $C_{[X,R]}$;
3. Set $\text{vec}(X^*) = M_R^{-1} \text{vec}(C_{[X,R]}^{\diamond*})$. This gives the solution to the least-squares problem in Eq. (2.16).

2.4 Special Cases

We now specialize the referenced deconvolution algorithm to three popular reference choices: the pinhole reference, the slit reference, and the (constant) block reference (see Fig. 4). The different choices lead to different M_R in step 3 of the algorithm. For all the three choices, the resulting M_R can be written as a Kronecker product of two simple matrices whose inverses are also explicit. We can hence obtain simple forms of M_R^{-1} taking advantage of the following fact.

Lemma 2.5 ([50]). *Suppose M_1 and M_2 are invertible. If $M = M_1 \otimes M_2$, then M is invertible and $M^{-1} = M_1^{-1} \otimes M_2^{-1}$. As well, if M_1 and M_2 are lower triangular Toeplitz, then M_1^{-1} and M_2^{-1} will also be lower triangular Toeplitz.*

Thus, suppose $M_R = M_1 \otimes M_2$ with both M_1 and M_2 invertible, $M_R^{-1} = M_1^{-1} \otimes M_2^{-1}$. Invoking Lemma 2.1 again, we conclude that step 3 of the above referenced deconvolution algorithm becomes

$$X^* = M_2^{-1} C_{[X,R]}^{\diamond*} (M_1^{-1})^\top. \quad (2.17)$$

2.4.1 Pinhole Reference

Definition 2.6. *The pinhole reference $R_p \in \mathbb{C}^{n \times n}$ is given by*

$$R_p(t_1, t_2) = \begin{cases} 1, & t_1 = t_2 = n - 1 \\ 0, & \text{otherwise.} \end{cases} \quad (2.18)$$

In this case, M_{R_p} is simply I_{n^2} (i.e., $I_n \otimes I_n$) and X is equal to $C_{[X,R]}^\diamond$. Our referenced deconvolution algorithm reduces to the non-iterative reconstruction procedure for Fourier holography [40]. The deconvolution procedure thus has $O(1)$ computational complexity.

2.4.2 Slit Reference

Definition 2.7. *The slit reference R_s (see, e.g., Fig. 4b) is given*

$$R_s(t_1, t_2) = \begin{cases} 1, & t_2 = n - 1 \\ 0, & \text{otherwise.} \end{cases} \quad (2.19)$$

Let $\mathbf{1}_L \in \mathbb{R}^{n \times n}$ be a lower-triangular matrix consisting of all ones on and below the main diagonal. It can be verified that

$$M_{R_s} = \text{diag}(\mathbf{1}_L, \dots, \mathbf{1}_L) = I_n \otimes \mathbf{1}_L. \quad (2.20)$$

The inverse of $\mathbf{1}_L$ is the first-order difference matrix [51]:

$$D_n(t_1, t_2) = \begin{cases} 1, & t_1 = t_2 \\ -1, & t_1 = t_2 - 1, \quad 1 \leq t_2 \leq n - 1 \\ 0, & \text{otherwise.} \end{cases} \quad (2.21)$$

Thus,

$$X^* = D_n C_{[X,R]}^{\diamond*}, \quad (2.22)$$

which only requires $O(n^2)$ operations thanks to the sparsity structure in D_n .

A natural interpretation of $D_n C_{[X,R]}^{\diamond*}$ is that one applies the finite-difference vertical differential operator D_n on the estimated cross-correlation $C_{[X,R]}^{\diamond*}$. This reproduces the recovery procedure for the slit reference proposed in [37]: D_n is exactly the finite-difference version of the directional derivative operator $\mathcal{L}^{(1)} \{ \cdot \}$ proposed in Section 4.1 of [37] for the vertical slit reference. The derivation in [37] depends on the derivative theorem for convolutions (Appendix A of [37]), and so one needs to assume beforehand the existence of a linear differential operator that solves the recovery problem.

2.4.3 Block Reference

Definition 2.8. The constant block reference R_b (see, e.g., Fig. 4c) is given by

$$R_b(t_1, t_2) = 1, \quad t_1, t_2 \in \{0, \dots, n-1\}. \quad (2.23)$$

The corresponding M_{R_b} is

$$M_{R_b} = \mathbf{1}_L \otimes \mathbf{1}_L \quad (2.24)$$

with inverse

$$M_{R_b}^{-1} = D_n \otimes D_n. \quad (2.25)$$

Thus,

$$X^* = D_n C_{[X,R]}^{\diamond\star} D_n^\top, \quad (2.26)$$

which again only requires $O(n^2)$ operations due to the sparsity structure in D_n .

Similar to the above, we can interpret $D_n C_{[X,R]}^{\diamond\star} D_n^\top$ as applying the finite-difference two-directional differential operator $D_n (\cdot) D_n^\top$ on the estimated cross-correlation $C_{[X,R]}^{\diamond\star}$. Again, this reproduces the recovery procedure for the constant block reference, which is a special parallelogram reference, proposed in Section 4.3 of [37]: $D_n (\cdot) D_n^\top$ is the finite-difference version of the two-directional directional derivative operator contained in equation (17) there.

3 Error Analysis and Comparison

Let Y^* be the possibly noisy data with the noise following a certain probability distribution, and let X^* be the estimate of the signal of interest returned by the referenced deconvolution algorithm described above, i.e., $\text{vec}(X^*) = T_R \text{vec}(Y^*)$, where T_R is as defined in Eq. (2.15). This linear relationship allows us to derive a general formula for the expected squared recovery error in Section 3.1. We further simplify the error formula for the three typical reference choices respectively in Section 3.2, based on which we obtain insights on their performances in Section 3.3.

3.1 Expected Error Formula

In dealing with complex-valued matrices, we use the standard Frobenius inner product as induced by the standard complex vector inner product.

Definition 3.1. For $B, C \in \mathbb{C}^{m \times m}$, their Frobenius (or, Hilbert-Schmidt) inner product is defined as $\langle B, C \rangle = \text{trace}(BC^*)$. Matrix Frobenius norm is induced by this inner product in a natural way: $\|B\|_F = (\langle B, B \rangle)^{1/2} = \left(\sum_{i,j} |B_{i,j}|^2 \right)^{1/2}$.

The following trace-shuffling identity is also useful for our subsequent calculation.

Lemma 3.2. For complex matrices B_1, B_2, C_1, C_2 of compatible dimensions, $\langle B_1 C_1, B_2 C_2 \rangle = \langle B_2^* B_1, C_2 C_1^* \rangle$.

A general formula for the expected squared recovery error follows simply from the trace-shuffling identity.

Lemma 3.3. The expected squared recovery error by referenced deconvolution is

$$\mathbb{E} \|X^* - X\|_F^2 = \langle T_R^* T_R, \mathbb{E} [\text{vec}(Y^*) - \text{vec}(Y)] [\text{vec}(Y^*) - \text{vec}(Y)]^* \rangle, \quad (3.1)$$

where for any given reference R , T_R is as defined in Eq. (2.15).

Proof. Direct calculation gives

$$\begin{aligned}
\mathbb{E} \|X^* - X\|_F^2 &= \mathbb{E} \|T_R \text{vec}(Y^*) - T_R \text{vec}(Y)\|_F^2 \\
&= \mathbb{E} \langle T_R \text{vec}(Y^*) - T_R \text{vec}(Y), T_R \text{vec}(Y^*) - T_R \text{vec}(Y) \rangle \\
&= \mathbb{E} \langle T_R^* T_R, [\text{vec}(Y^*) - \text{vec}(Y)] [\text{vec}(Y^*) - \text{vec}(Y)]^* \rangle \\
&= \langle T_R^* T_R, \mathbb{E} [\text{vec}(Y^*) - \text{vec}(Y)] [\text{vec}(Y^*) - \text{vec}(Y)]^* \rangle,
\end{aligned}$$

as claimed. \blacksquare

This formula provides a very reasonable design target: given X and the noise model, one can seek a reference choice R which minimizes the expected squared error. This may be difficult in general, but the perspective forms the basis of our subsequent analysis.

We now specialize the analysis assuming a Poisson shot noise model on the data [52]. Poisson shot noise occurs in any experiment in which photons are collected. It is an inherent feature of the quantum nature of photon emission, and cannot be removed by any physical apparatus [52]. The model can be described as follows. Let N_p be the expected (or nominal) number of photons reaching the detector. Given the squared Fourier transform magnitudes $Y = |\widehat{[X, R]}|^2$, let

$$\|Y\|_1 \doteq \sum_{k_1, k_2=0}^{m-1} Y(k_1, k_2). \quad (3.2)$$

Then, the photon flux at the (k_1, k_2) -th pixel location is given by a Poisson distribution with parameter $N_p Y(k_1, k_2) / \|Y\|_1$ and then scaled by $\|Y\|_1 / N_p$. These pixel distributions are also assumed to be jointly independent [46]. We thus have the data given by

$$Y^* \sim_{\text{ind}} \frac{\|Y\|_1}{N_p} \text{Pois}\left(\frac{N_p}{\|Y\|_1} Y\right). \quad (3.3)$$

We now apply this noise model to Eq. (3.1). Recall that both the mean and variance of a Poisson-distributed random variable with parameter λ are equal to λ . It then follows that

$$\begin{aligned}
\mathbb{E} [\text{vec}(Y^*) - \text{vec}(Y)] [\text{vec}(Y^*) - \text{vec}(Y)]^* &= \frac{\|Y\|_1^2}{N_p^2} \times \frac{N_p}{\|Y\|_1} \text{diag}(\text{vec}(Y)) \\
&= \frac{\|Y\|_1}{N_p} \text{diag}(\text{vec}(Y)).
\end{aligned}$$

Hence,

$$\mathbb{E} \|X^* - X\|_F^2 = \left\langle T_R^* T_R, \frac{\|Y\|_1}{N_p} \text{diag}(\text{vec}(Y)) \right\rangle = \frac{\|Y\|_1}{N_p} \langle S_R, Y \rangle, \quad (3.4)$$

where $S_R = \text{reshape}(\text{diag}(T_R^* T_R), m, m)$, and $\text{reshape}(\cdot, m, m)$ is the columnwise vector-to-matrix reshaping operator. In other words, the expected squared recovery error is proportional to the weighted sum of the squared frequency values in Y , where the weights are determined by S_R .

It is possible to derive a (conservative) uniform lower bound on S_R for all references; later we will use the result to compare the relative performance of different references.

Lemma 3.4. *For all reference choices R (with entry magnitudes normalized within $[0, 1]$), and for all $k_1, k_2 \in \{0, \dots, m-1\}$,*

$$S_R(k_1, k_2) \geq \frac{1}{m^4}. \quad (3.5)$$

Proof. For all $k_1, k_2 \in \{0, \dots, m-1\}$ and the corresponding $k = mk_1 + k_2$,

$$\begin{aligned}
S_R(k_1, k_2) &= (T_R^* T_R)(k, k) \\
&= \sum_{t=0}^{n^2-1} |T_R(t, k)|^2 \\
&= |T_R(0, k)|^2 + \sum_{t=1}^{n^2-1} |T_R(t, k)|^2 \\
&= \frac{1}{m^4} \left| (M_R^{-1} [(P_2 F_{RA}^*) \otimes (P_1 F_{LA}^*)]) (0, k) \right|^2 + \sum_{t=1}^{n^2-1} |T_R(t, k)|^2.
\end{aligned}$$

By [Lemma 2.5](#), M_R^{-1} is lower triangular. So $(M_R^{-1} [(P_2 F_{RA}^*) \otimes (P_1 F_{LA}^*)]) (0, k)$ is equal to the product of $M_R^{-1}(0, 0)$, and the first element of the k -th column of $(P_2 F_{RA}^*) \otimes (P_1 F_{LA}^*)$ which takes the form $e^{i\theta}$ for a certain θ . Thus,

$$\left| (M_R^{-1} [(P_2 F_{RA}^*) \otimes (P_1 F_{LA}^*)]) (0, k) \right|^2 = \left| M_R^{-1}(0, 0) \right|^2 \geq 1, \quad (3.6)$$

where the last inequality holds, as we assume $M_R(0, 0) \in [0, 1]$. This completes the proof. \blacksquare

3.2 Special Cases

Note that only the diagonal entries of $T_R^* T_R$, i.e., squared column norms of T_R , come into play in [Eq. \(3.4\)](#),² and thus there is no need to perform full computation of $T_R^* T_R$. Note that T_R takes the form of $B_1 \otimes B_2$ for certain B_1 and B_2 , which motivates the following result.

Lemma 3.5. Suppose $B_1 \in \mathbb{C}^{n_1 \times m_1}$, $B_2 \in \mathbb{C}^{n_2 \times m_2}$, and $B = B_1 \otimes B_2 \in \mathbb{C}^{n_1 n_2 \times m_1 m_2}$. Then, for $k_1 \in \{0, \dots, m_1\}$, $k_2 \in \{0, \dots, m_2\}$, and $k = m_2 k_1 + k_2 \in \{0, \dots, m_1 m_2 - 1\}$, it holds that

$$\|B(:, k)\|^2 = \|B_1(:, k_1)\|^2 \|B_2(:, k_2)\|^2,$$

where we use MATLAB notation $(:, k)$ and alike to index matrix columns.

Proof. By the definition of Kronecker product,

$$B(:, k) = \begin{bmatrix} B_1(0, k_1) B_2(:, k_2) \\ B_1(1, k_1) B_2(:, k_2) \\ \vdots \\ B_1(n_1, k_1) B_2(:, k_2) \end{bmatrix}.$$

Thus,

$$\|B(:, k)\|^2 = \sum_{t=0}^{n_1} |B_1(t, k_1)|^2 \|B_2(:, k_2)\|^2 = \|B_2(:, k_2)\|^2 \sum_{t=0}^{n_1} |B_1(t, k_1)|^2 = \|B_2(:, k_2)\|^2 \|B_1(:, k_1)\|^2,$$

as claimed. \blacksquare

Next, we make use of the result to calculate the expected recovery errors of the special references as introduced in [Section 2.4](#).

²This holds true so long as the observation noise is jointly independent across the magnitude observations.

3.2.1 Pinhole Reference

Proposition 3.6. Let R_p denote the pinhole reference given by Definition 2.6. For $k_1, k_2 \in \{0, \dots, m-1\}$,

$$S_{R_p}(k_1, k_2) = \frac{n^2}{m^4}. \quad (3.7)$$

Proof. Since $M_{R_p} = I_{n^2}$, by Eq. (2.14), we have that

$$T_{R_p} = \frac{1}{m^2} (P_2 F_{RA}^*) \otimes (P_1 F_{LA}^*).$$

By Lemma 3.5, for any $k_1, k_2 \in \{0, \dots, m-1\}$ and $k = mk_1 + k_2$,

$$\|T_{R_p}(:, k)\|^2 = \frac{1}{m^4} \|(P_2 F_{RA}^*)(:, k_1)\|^2 \|(P_1 F_{LA}^*)(:, k_2)\|^2.$$

Observe that any element in $P_2 F_{RA}^*$ or $P_1 F_{LA}^*$ has a unit norm, we conclude that

$$\|(P_2 F_{RA}^*)(:, k_1)\|^2 = \|(P_1 F_{LA}^*)(:, k_2)\|^2 = n,$$

implying the claimed result. ■

3.2.2 Slit Reference

Proposition 3.7. Let R_s denote the slit reference given by Definition 2.7. For $k_1, k_2 \in \{0, \dots, m-1\}$,

$$S_{R_s}(k_1, k_2) = \frac{n}{m^4} [1 + 2(n-1)(1 - \cos(2\pi k_2/m))].$$

Proof. By the discussion below Definition 2.7,

$$M_{R_s}^{-1} = I_n \otimes D_n,$$

where D_n is the first-order difference matrix defined in Eq. (2.21). So by Eq. (2.14),

$$T_{R_s} = \frac{1}{m^2} [I_n \otimes D_n] ((P_2 F_{RA}^*) \otimes (P_1 F_{LA}^*)) = (P_2 F_{RA}^*) \otimes (D_n P_1 F_{LA}^*),$$

where at last equality we have used the mixed-product property³ of the Kronecker product.

By Lemma 3.5, for any $k_1, k_2 \in \{0, \dots, m-1\}$ and $k = mk_1 + k_2$,

$$\|T_{R_s}(:, k)\|^2 = \frac{1}{m^4} \|(P_2 F_{RA}^*)(:, k_1)\|^2 \|(D_n P_1 F_{LA}^*)(:, k_2)\|^2.$$

Per the proof of Proposition 3.6, $\|(P_2 F_{RA}^*)(:, k_1)\|^2 = n$. For the other term,

$$\begin{aligned} \|(D_n P_1 F_{LA}^*)(:, k_2)\|^2 &= \|D_n P_1 [F_{LA}^*(:, k_2)]\|^2 \\ &= \left\| D_n \begin{bmatrix} e^{-2\pi i(n-1)k_2/m} \\ e^{-2\pi i(n-2)k_2/m} \\ \vdots \\ e^{2\pi i 0 k_2/m} \end{bmatrix} \right\|^2 \\ &= 1 + \sum_{t=1}^{n-1} \left| e^{-2\pi i t k_2/m} - e^{-2\pi i (t-1)k_2/m} \right|^2 \\ &= 1 + \sum_{t=1}^{n-1} (2 - 2 \cos(2\pi k_2/m)) \\ &= 1 + 2(n-1)(1 - \cos(2\pi k_2/m)), \end{aligned}$$

completing the proof. ■

³See, e.g., the third property under the “properties” section of this Wikipedia article https://en.wikipedia.org/wiki/Kronecker_product.

3.2.3 Block Reference

Proposition 3.8. Let R_b denote the block reference given by [Definition 2.8](#). For $k_1, k_2 \in \{0, \dots, m-1\}$,

$$S_{R_b}(k_1, k_2) = \frac{1}{m^4} [1 + 2(n-1)(1 - \cos(2\pi k_1/m))] [1 + 2(n-1)(1 - \cos(2\pi k_2/m))]. \quad (3.8)$$

Proof. As shown in [Eq. \(2.25\)](#),

$$M_{R_b}^{-1} = D_n \otimes D_n.$$

After applying the mixed-product property of the Kronecker product and also [Lemma 3.5](#) analogous to the above proof of the slit reference, it is clear that we only have to calculate $\|(D_n P_1 F_{L_A}^*)(:, k_2)\|^2$ and $\|(D_n P_2 F_{R_A}^*)(:, k_1)\|^2$. Performing analogous calculation as in the slit case completes the proof. ■

3.3 Reference Design Optimality

For a fixed specimen X , we may view the recovery error given by [Eq. \(3.4\)](#) as an objective (i.e. cost) function whose variables are the reference values. From this perspective, each of the special cases considered exhibits a unique characteristic, as we discuss below.

In [Eq. \(3.4\)](#), both $Y = \|\widehat{[X, R]}\|^2$ and S_R depend on the reference R , and both Y and S_R contribute to the expected error.

- For Y , note that

$$\|\widehat{[X, R]}\|^2 = \|\widehat{[X, 0]} + \widehat{[0, R]}\|^2 \quad (\text{Fourier transform is a linear operator}) \quad (3.9)$$

$$= \|\widehat{[X, 0]}\|^2 + \|\widehat{[0, R]}\|^2 + 2\Re(\widehat{[X, 0]} \odot \widehat{[0, R]}), \quad (3.10)$$

where \odot denotes the elementwise Hadamard product. Here $\widehat{[X, 0]}$ and $\widehat{[0, R]}$ are horizontally-oversampled Fourier transforms of X and R , respectively, with certain phase modifications. Moreover,

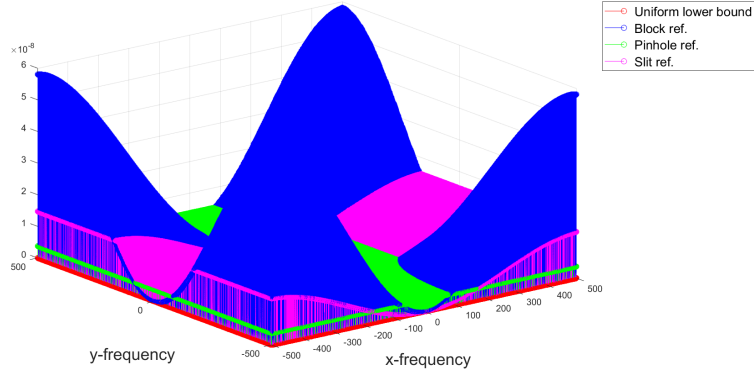
$$\|Y\|_1 = \|\widehat{[X, R]}\|^2 = m^2 \|[X, R]\|^2 = m^2 \|X\|^2 + m^2 \|R\|^2, \quad (3.11)$$

where the second equality follows from Parseval's theorem.

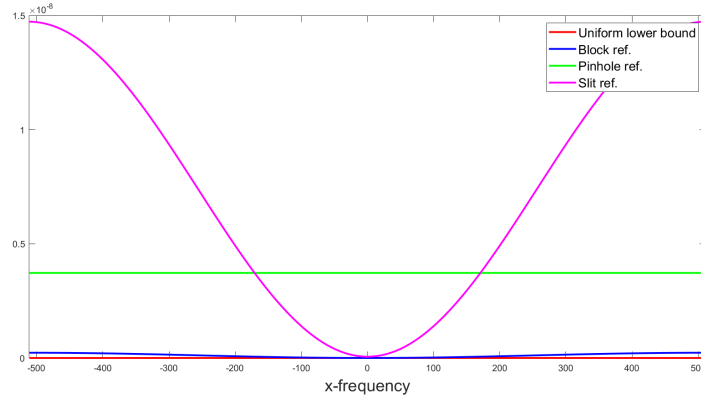
- The S_R term changes significantly across the references: for example, on a 64×64 image, the zero-frequency scaling term $S_R(0, 0)$ for the block reference is $1/64$ of that for the slit reference, and is $1/64^2$ of that for the pinhole reference, as implied by [Propositions 3.6 to 3.8](#). By [Proposition 3.6](#), the pinhole reference induces a “flat” weighting scheme with a uniform weight n^2/m^4 . By contrast, the weights induced by the block reference are frequency-varying ([Proposition 3.8](#)): when one of k_1 and k_2 is reasonably small, the weights are on the order $O(n/m^4)$, and when both are small, the weights are on the optimal order $O(1/m^4)$, which matches the lower bound given by [Lemma 3.4](#). The weights induced by the slit reference interpolate the previous two in different directions: for a fixed k_2 , the weight is constant and the behavior matches that of the pinhole reference, whereas the behavior is similar to that of the block reference when k_2 changes. The weighting behaviors of the three references are demonstrated in [Fig. 7](#).

To illustrate how [Eq. \(3.4\)](#) and the above facts can help provide insights into reference design and choice, we look at two stylized cases. For this discussion, reference choice is confined to the three special references we discussed above.

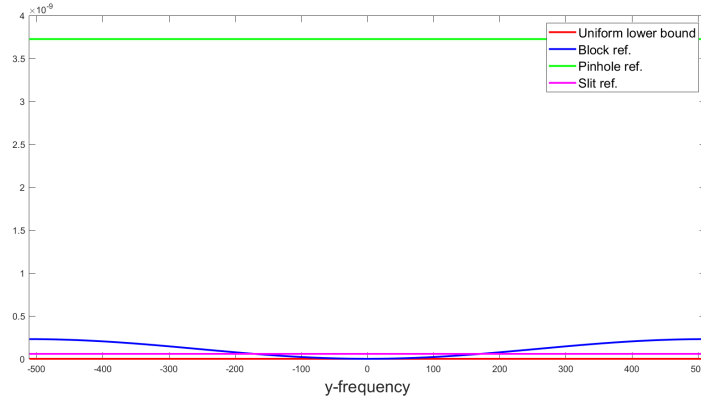
- **Case I: Spectrum of X concentrates on (super) low-frequency bands.** A good example is when $X = \mathbf{1}_{n \times n}$. We think of X as “flat” and has values on the order of $\Theta(1)$. So $\|X\|^2 \in \Theta(n^2)$. Then



(a)



(b)



(c)

Figure 7: Plot of S_R for the three special references and the uniform lower bound established in [Lemma 3.4](#). [Fig. 7a](#) shows the entire frequency spectrum (i.e., across all (k_1, k_2)), and [Fig. 7b](#) and [Fig. 7c](#) show the cross-sections cutting the origin and parallel to the x and y directions, respectively. While the pinhole reference induces a flat scaling to the entire spectrum (as predicted in [Proposition 3.6](#)), the values for the block references are small at the low frequencies, and grow toward larger values moving into high frequencies. The slit reference interpolates the behaviors across directions: along the y -axis, the values are constant—same as the pinhole reference, but along the x -axis, the value increases as the frequency grows, similar to the block reference.

whatever the choice of R , $\|X\|^2 + \|R\|^2 \in \Theta(n^2)$. So the contribution by $\|Y\|_1$ only differs across the three references by a small constant factor. Moreover, by Eq. (3.9), Y is low-frequency dominant regardless of the reference. According to our above discussion about the weight distribution of S_R , using the block reference might be beneficial for this class of signals (depending on of course how concentrated the low-frequency components of Y is).

- **Case II: Spectrum of X is flat or has significant medium- to high-frequency components.** A contrived example is when $X = \delta(0, 0)$. For these signals, $\langle Y, S_R \rangle$ are roughly the same whether we choose the block or the pinhole reference: for the block reference, the n^2 factor introduced by $\widehat{[0, R]}$ into the low-frequency components of Y is countered by the $1/n^2$ (lower) factor in S_R , and the weights for medium- to high-frequency components of the two are on the same order. So the final performance of the two largely depends on $\|Y\|_1$. When $\|X\|^2 \in \Theta(n^2)$, we do not expect substantial differences. When $\|X\| \in o(n^2)$, say $\|X\| = 1$ (for $\delta(0, 0)$), obviously the pinhole reference is more favorable, as $\|R_p\|^2 = 1$ whereas $\|R_b\|^2 = n^2$.

It is natural to expect a smooth transition of the behaviors moving from the super-flat signal **1** to the super sharp $\delta(0, 0)$. We confirm the differential behaviors of the references empirically in Section 4.

4 Numerical Simulations

We perform numerical experiments on two sets of data to illustrate the effectiveness of the referenced deconvolution algorithm (Section 2.3), and to corroborate the theoretical prediction on optimal reference design (Section 3.3). Code for these experiments is available at https://github.com/sunju/REF_CDI.

4.1 On the Mimivirus Image

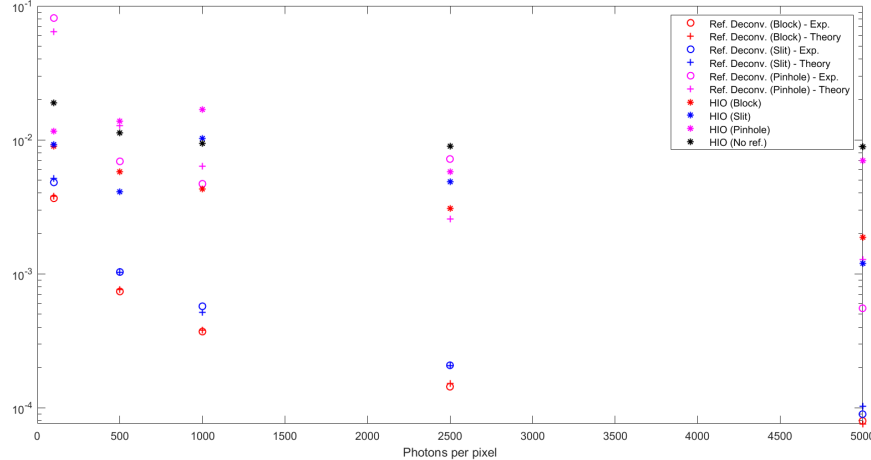


Figure 8: Plot of the relative recovery error against the nominal photon level for experiments on the mimivirus image. Result from both the referenced deconvolution and the classic HIO algorithms are included; for the referenced deconvolution algorithm, both the expected and empirical recovery errors are presented. The reference deconvolution algorithm combined with the block reference performs consistently better than other algorithm-reference combinations. Also, for each reference, the expected recovery error agrees with the empirical recovery error.

In this experiment, the specimen X is the mimivirus image [34], and its spectrum mostly concentrates on very low frequencies, as shown in Fig. 10b. The image size is 64×64 , and the pixel values are normalized to

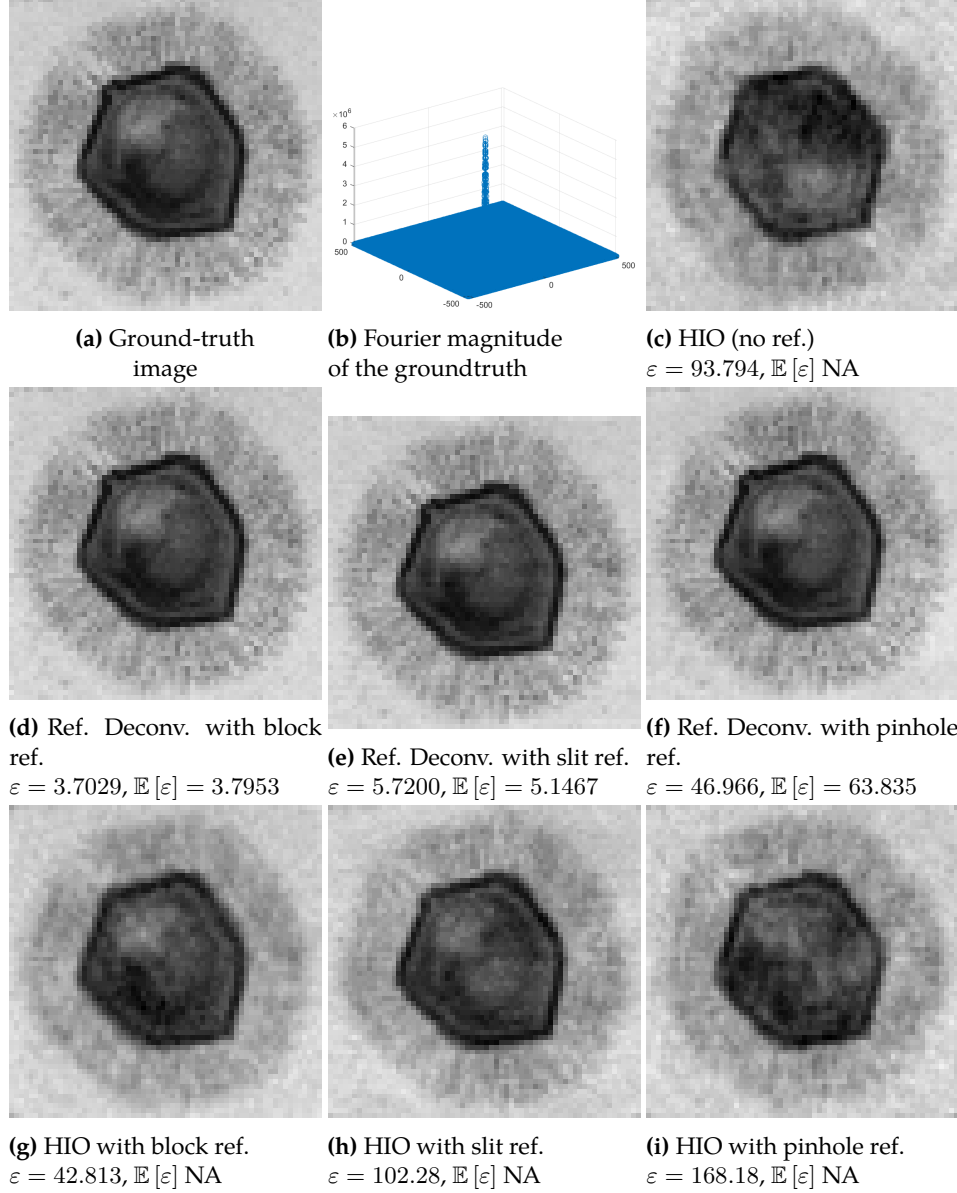


Figure 9: Recovery result of the mimivirus image using various recovery schemes, and the corresponding relative recovery errors (**all errors should be rescaled by 10^{-4}**). The photon level N_{pp} is fixed as 1000. Referenced deconvolution achieves superior recovery to HIO (with the reference information enforced). Experimental and theoretical relative errors for referenced deconvolution closely match. The block reference achieves the best recovery.

$[0, 1]$. For the reference setup, a reference R of size 64×64 is placed next to X , forming a composite specimen $[X, R]$ of size 64×128 . Three references, i.e., the pinhole, the slit, and the block references are considered. The oversampled Fourier transform is taken to be of size 1024×1024 , and the collected noisy data Y^* obeys the Poisson shot noise model defined in Eq. (3.3). For this model, the nominal number of total photons N_p is given by $N_{pp} \times 1024^2$, where N_{pp} can be understood to be the average number of photons to be received by each pixel. We investigate the regime where N_{pp} varies from 100 to 5000 ($N_{pp} = 100, 500, 1000, 2500, 5000$, respectively).

We run the referenced deconvolution algorithm and also the classic HIO algorithm with and without enforcing the known reference for comparison. The results are presented in Fig. 8 and Fig. 9. We define the relative (squared) recovery error to be

$$\varepsilon \doteq \frac{\|X - X^*\|^2}{\|X\|^2}. \quad (4.1)$$

From Fig. 8, it is evident that for the referenced deconvolution schemes, the expected and empirical relative recovery errors are close. Moreover, referenced deconvolution combined with the block reference performs the best among all the schemes—across referenced deconvolution and HIO combined with all three references—regardless of the photon per pixel level N_{pp} . The superiority of the block reference among the referenced deconvolution schemes agrees with the prediction in Section 3.3, as spectrum of X sharply concentrates on very low frequencies. In addition, for the referenced deconvolution schemes, the recovery errors generally decrease as the photon level (dictated by N_{pp}) increases. This trend is clearly predicted by Eq. (3.4): because only $N_p = N_{pp} \times 1024^2$ depends on N_{pp} , the expected squared error is proportional to $1/N_{pp}$. The detailed performance scores and recovered images for $N_{pp} = 1000$ are exhibited in Fig. 9.

4.2 On a ‘Flat-Spectrum’ Image

In this experiment, the image contains a small centered square. Except for this, the basic experimental setup is identical to the above one. We focus on the case $N_{pp} = 1000$. In terms of recovery error, the referenced deconvolution schemes perform uniformly better than the HIO schemes, same as our observation for the mimivirus image. For the current “centered square” image which has a considerably “flat” spectrum (see Fig. 10b), however, the best-performing reference is the pinhole reference—again consistent with our theoretical prediction in Section 3.3. The detailed recovery results and recovery errors are presented in Fig. 10.

5 Discussion

We have presented a general mathematical framework for the holographic phase retrieval problem, and proposed the referenced deconvolution algorithm as a generic method for solving the problem. Our formulation emphasizes the structure in the linear deconvolution procedure, and offers new insights into the resulting linear systems from popular reference choices.

We have also derived a general formula for the expected recovery error of the referenced deconvolution algorithm when the measurement data contains stochastic noise. Under a Poisson shot noise model, the formula allows us to compare popular reference choices and conclude that the block reference minimizes low-frequency contributions to the recovery error and is hence favorable for typical imaging data.

Building on our framework, it is possible to perform more detailed analysis of other noise model and reference choices. Also, the insights obtained here can likely motivate further design possibilities.

Another possible extension is to include beam stop, which is often implemented in practical CDI experiments [37, 53]. Beam stop effectively removes a small fraction ($\leq 5\%$) of low-frequency components from the measurements. We observe that the proposed referenced deconvolution algorithm is easily adapted to this setting, insofar as the missing data does not render the problem ill-conditioned.

6 Acknowledgments

The authors are grateful to the Simons Foundation Math+X initiative and the Natural Science and Engineering Research Council of Canada for providing support during our study. We would also like to sincerely thank Walter Murray and Gordon Wetzstein for ongoing valuable feedback towards developing this work.

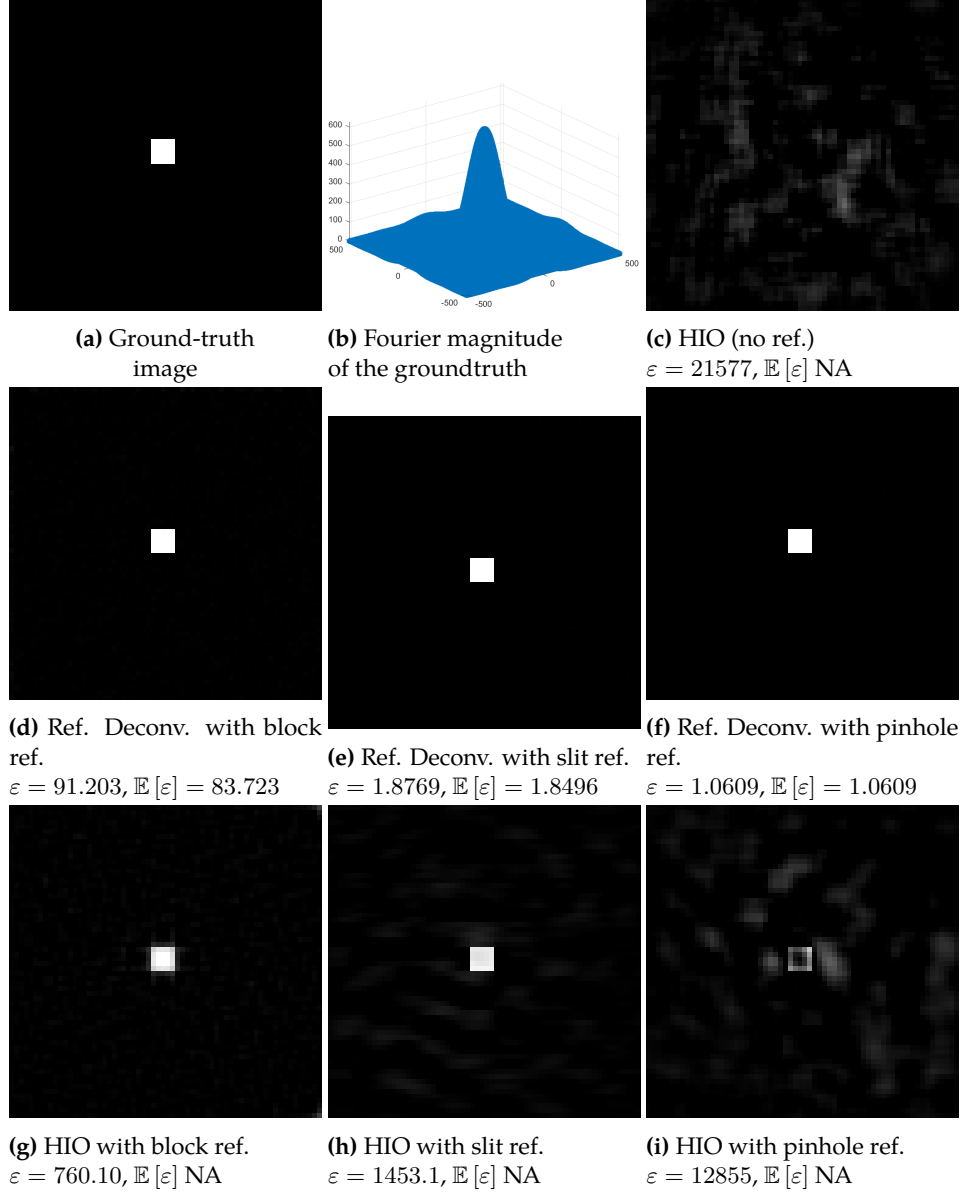


Figure 10: Recovery result of the “centered square” image using various recovery schemes, and the corresponding relative recovery errors (**all errors should be rescaled by 10^{-4}**). The photon level N_{pp} is fixed as 1000. Referenced deconvolution achieves superior recovery to HIO (with the reference information enforced). Experimental and theoretical relative errors for referenced deconvolution closely match. The pinhole reference achieves the best recovery.

References

- [1] R. P. Millane, “Phase retrieval in crystallography and optics,” *J. Opt. Soc. Am. A*, vol. 7, no. 3, pp. 394–411, mar 1990. [Online]. Available: <http://josaa.osa.org/abstract.cfm?URI=josaa-7-3-394>
- [2] O. Bunk, A. Diaz, F. Pfeiffer, C. David, B. Schmitt, D. K. Satapathy, and J. F. van der Veen, “Diffractive imaging for periodic samples: retrieving one-dimensional concentration profiles across microfluidic

- channels," *Acta Crystallographica Section A*, vol. 63, no. 4, pp. 306–314, jul 2007. [Online]. Available: <https://doi.org/10.1107/S0108767307021903>
- [3] A. Walther, "The question of phase retrieval in optics," *Optica Acta: International Journal of Optics*, vol. 10, no. 1, pp. 41–49, 1963.
- [4] J. C. Dainty and J. R. Fienup, "Phase retrieval and image reconstruction for astronomy," in *Image Recovery: Theory and Application*, H. Stark, Ed. Academic Press, 1987.
- [5] J. Miao, P. Charalambous, J. Kirz, and D. Sayre, "Extending the methodology of X-ray crystallography to allow imaging of micrometre-sized non-crystalline specimens," *Nature*, vol. 400, pp. 342–344, jul 1999.
- [6] J. W. Goodman, *Introduction to Fourier Optics*, 4th ed. New York, NY, USA: Macmillan Learning, 2017.
- [7] K. Jaganthan, "Convex programming-based phase retrieval: Theory and applications," 2016.
- [8] Y. Shechtman, Y. C. Eldar, O. Cohen, H. N. Chapman, J. Miao, and M. Segev, "Phase retrieval with application to optical imaging: a contemporary overview," *IEEE signal processing magazine*, vol. 32, no. 3, pp. 87–109, 2015.
- [9] H. N. Chapman, A. Barty, M. J. Bogan, S. Boutet, M. Frank, S. P. Hau-Riege, S. Marchesini, B. W. Woods, S. Bajt, W. H. Benner, R. A. London, E. Plönjes, M. Kuhlmann, R. Treusch, S. Düsterer, T. Tschentscher, J. R. Schneider, E. Spiller, T. Möller, C. Bostedt, M. Hoener, D. A. Shapiro, K. O. Hodgson, D. van der Spoel, F. Burmeister, M. Bergh, C. Caleman, G. Huldt, M. M. Seibert, F. R. N. C. Maia, R. W. Lee, A. Szöke, N. Timneanu, and J. Hajdu, "Femtosecond diffractive imaging with a soft-X-ray free-electron laser," *Nature Physics*, vol. 2, pp. 839–843, nov 2006.
- [10] I. K. Robinson, I. A. Vartanyants, G. J. Williams, M. A. Pfeifer, and J. A. Pitney, "Reconstruction of the Shapes of Gold Nanocrystals Using Coherent X-Ray Diffraction," *Phys. Rev. Lett.*, vol. 87, no. 19, p. 195505, oct 2001. [Online]. Available: <https://link.aps.org/doi/10.1103/PhysRevLett.87.195505>
- [11] Y. H. Lo, L. Zhao, M. Gallagher-Jones, A. Rana, J. J. Lodico, W. Xiao, B. C. Regan, and J. Miao, "In situ coherent diffractive imaging," *Nature Communications*, vol. 9, no. 1, p. 1826, 2018.
- [12] G. Xiong, O. Moutanabbir, M. Reiche, R. Harder, and I. Robinson, "Coherent X-Ray Diffraction Imaging and Characterization of Strain in Silicon-on-Insulator Nanostructures," *Advanced Materials*, vol. 26, no. 46, pp. 7747–7763, 2014. [Online]. Available: <https://onlinelibrary.wiley.com/doi/abs/10.1002/adma.201304511>
- [13] N. D. Loh, C. Y. Hampton, A. V. Martin, D. Starodub, R. G. Sierra, A. Barty, A. Aquila, J. Schulz, L. Lomb, J. Steinbrener, R. L. Shoeman, S. Kassemeyer, C. Bostedt, J. Bozek, S. W. Epp, B. Erk, R. Hartmann, D. Rolles, A. Rudenko, B. Rudek, L. Foucar, N. Kimmel, G. Weidenspointner, G. Hauser, P. Holl, E. Pedersoli, M. Liang, M. S. Hunter, L. Gumprecht, N. Coppola, C. Wunderer, H. Graafsma, F. R. N. C. Maia, T. Ekeberg, M. Hantke, H. Fleckenstein, H. Hirsemann, K. Nass, T. A. White, H. J. Tobias, G. R. Farquar, W. H. Benner, S. P. Hau-Riege, C. Reich, A. Hartmann, H. Soltau, S. Marchesini, S. Bajt, M. Barthelmess, P. Bucksbaum, K. O. Hodgson, L. Strüder, J. Ullrich, M. Frank, I. Schlichting, H. N. Chapman, and M. J. Bogan, "Fractal morphology, imaging and mass spectrometry of single aerosol particles in flight," *Nature*, vol. 486, pp. 513–517, jun 2012.
- [14] J. Miao, T. Ishikawa, I. K. Robinson, and M. M. Murnane, "Beyond crystallography: Diffractive imaging using coherent x-ray light sources," *Science*, vol. 348, no. 6234, pp. 530–535, 2015. [Online]. Available: <http://science.sciencemag.org/content/348/6234/530>
- [15] E. J. Candès, X. Li, and M. Soltanolkotabi, "Phase retrieval from coded diffraction patterns," *Applied and Computational Harmonic Analysis*, vol. 39, no. 2, pp. 277–299, 2015. [Online]. Available: <http://www.sciencedirect.com/science/article/pii/S1063520314001201>

- [16] M. Hayes, "The reconstruction of a multidimensional sequence from the phase or magnitude of its Fourier transform," *IEEE Transactions on Acoustics, Speech, and Signal Processing*, vol. 30, no. 2, pp. 140–154, apr 1982.
- [17] T. Bendory, R. Beinert, and Y. C. Eldar, *Fourier Phase Retrieval: Uniqueness and Algorithms*. Cham: Springer International Publishing, 2017. [Online]. Available: https://doi.org/10.1007/978-3-319-69802-1_2
- [18] K. G. Murty and S. N. Kabadi, "Some np-complete problems in quadratic and nonlinear programming," *Mathematical Programming*, vol. 39, no. 2, pp. 117–129, Jun 1987. [Online]. Available: <https://doi.org/10.1007/BF02592948>
- [19] J. R. Fienup, "Reconstruction of an object from the modulus of its Fourier transform," *Opt. Lett.*, vol. 3, no. 1, pp. 27–29, jul 1978. [Online]. Available: <http://ol.osa.org/abstract.cfm?URI=ol-3-1-27>
- [20] D. R. Luke, "Relaxed averaged alternating reflections for diffraction imaging," *Inverse Problems*, vol. 21, no. 1, pp. 37–50, 2005.
- [21] V. Elser, I. Rankenburg, and P. Thibault, "Searching with iterated maps," *Proceedings of the National Academy of Sciences*, vol. 104, no. 2, pp. 418–423, 2007. [Online]. Available: <http://www.pnas.org/content/104/2/418>
- [22] Z. Wen, C. Yang, X. Liu, and S. Marchesini, "Alternating direction methods for classical and ptychographic phase retrieval," *Inverse Problems*, vol. 28, no. 11, p. 115010, 2012.
- [23] S. Boyd, N. Parikh, E. Chu, B. Peleato, and J. Eckstein, "Distributed optimization and statistical learning via the alternating direction method of multipliers," *Found. Trends Mach. Learn.*, vol. 3, no. 1, pp. 1–122, Jan. 2011. [Online]. Available: <http://dx.doi.org/10.1561/22000000016>
- [24] D. Barmherzig and J. Sun, "A Local Analysis of Block Coordinate Descent for Gaussian Phase Retrieval," *10th NIPS Workshop on Optimization for Machine Learning*, vol. abs/1712.0, 2017. [Online]. Available: <http://arxiv.org/abs/1712.02083>
- [25] S. Marchesini, "Invited article: A unified evaluation of iterative projection algorithms for phase retrieval," *Review of scientific instruments*, vol. 78, no. 1, p. 11301, 2007.
- [26] V. Elser, "Phase retrieval by iterated projections," *J. Opt. Soc. Am. A*, vol. 20, no. 1, pp. 40–55, jan 2003. [Online]. Available: <http://josaa.osa.org/abstract.cfm?URI=josaa-20-1-40>
- [27] Y. J. Liu, B. Chen, E. R. Li, J. Y. Wang, A. Marcelli, S. W. Wilkins, H. Ming, Y. C. Tian, K. A. Nugent, P. P. Zhu, and Z. Y. Wu, "Phase retrieval in x-ray imaging based on using structured illumination," *Phys. Rev. A*, vol. 78, p. 023817, Aug 2008. [Online]. Available: <https://link.aps.org/doi/10.1103/PhysRevA.78.023817>
- [28] I. Johnson, K. Jefimovs, O. Bunk, C. David, M. Dierolf, J. Gray, D. Renker, and F. Pfeiffer, "Coherent diffractive imaging using phase front modifications," *Phys. Rev. Lett.*, vol. 100, p. 155503, Apr 2008. [Online]. Available: <https://link.aps.org/doi/10.1103/PhysRevLett.100.155503>
- [29] K. Jaganathan, Y. Eldar, and B. Hassibi, "Phase retrieval with masks using convex optimization," in *2015 IEEE International Symposium on Information Theory (ISIT)*, June 2015, pp. 1655–1659.
- [30] K. Jaganathan, Y. C. Eldar, and B. Hassibi, "Phase retrieval: an overview of recent developments," pp. 263–296, 2016.
- [31] E. J. Candès, X. Li, and M. Soltanolkotabi, "Phase retrieval via wirtinger flow: Theory and algorithms," *IEEE Trans. Inf. Theory*, vol. 61, no. 4, pp. 1985–2007, Apr. 2015.
- [32] D. Gabor, "A New Microscopic Principle," *Nature*, vol. 161, pp. 777–778, may 1948.

- [33] M. Saliba, T. Latychevskaia, J. Longchamp, and H. Fink, "Fourier Transform Holography: A Lensless Non-Destructive Imaging Technique," *Microscopy and Microanalysis*, vol. 18, no. S2, pp. 564–565, 2012.
- [34] E. Ghigo, J. Kartenbeck, P. Lien, L. Pelkmans, C. Capo, J.-L. Mege, and D. Raoult, "Ameobal Pathogen Mimivirus Infects Macrophages through Phagocytosis," *PLOS Pathogens*, vol. 4, no. 6, pp. 1–17, 2008. [Online]. Available: <https://doi.org/10.1371/journal.ppat.1000087>
- [35] S. Kikuta, S. Aoki, S. Kosaki, and K. Kohra, "X-ray holography of lensless Fourier-transform type," *Optics Communications*, vol. 5, no. 2, pp. 86–89, 1972. [Online]. Available: <http://www.sciencedirect.com/science/article/pii/0030401872900053>
- [36] S. Eisebitt, J. L  ening, W. F. Schlotter, M. L  tgen, O. Hellwig, W. Eberhardt, and J. St  hr, "Lensless imaging of magnetic nanostructures by X-ray spectro-holography," *Nature*, vol. 432, pp. 885–888, dec 2004.
- [37] M. Guizar-Sicairos and J. R. Fienup, "Holography with extended reference by autocorrelation linear differential operation," *Opt. Express*, vol. 15, no. 26, pp. 17 592–17 612, dec 2007. [Online]. Available: <http://www.opticsexpress.org/abstract.cfm?URI=oe-15-26-17592>
- [38] A. V. Martin and L. J. Allen, "Direct retrieval of a complex wave from its diffraction pattern," *Optics Communications*, vol. 281, no. 20, pp. 5114–5121, 2008. [Online]. Available: <http://www.sciencedirect.com/science/article/pii/S0030401808006664>
- [39] T. Gorkhover and Others, "Femtosecond X-ray Fourier holography imaging of free-flying nanoparticles," *Nature Photonics*, vol. 12, no. 3, pp. 150–153, 2018. [Online]. Available: <https://doi.org/10.1038/s41566-018-0110-y>
- [40] E. N. Leith and J. Upatnieks, "Reconstructed wavefronts and communication theory," *Journal of the Optical Society of America*, vol. 52, no. 10, pp. 1123–1130, 1962.
- [41] M. Guizar-Sicairos and J. R. Fienup, "Direct image reconstruction from a Fourier intensity pattern using HERALDO," *Opt. Lett.*, vol. 33, no. 22, pp. 2668–2670, nov 2008. [Online]. Available: <http://ol.osa.org/abstract.cfm?URI=ol-33-22-2668>
- [42] D. Zhu and Others, "High-resolution X-ray lensless imaging by differential holographic encoding," *Physical review letters*, vol. 105, no. 4, p. 43901, 2010.
- [43] S. G. Podorov, K. M. Pavlov, and D. M. Paganin, "A non-iterative reconstruction method for direct and unambiguous coherent diffractive imaging," *Opt. Express*, vol. 15, no. 16, pp. 9954–9962, aug 2007. [Online]. Available: <http://www.opticsexpress.org/abstract.cfm?URI=oe-15-16-9954>
- [44] D. Barmherzig, J. Sun, P.-N. Li, and T. J. Lane, "On Block-Reference Coherent Diffraction Imaging," in *Imaging and Applied Optics 2018 (3D, AO, AIO, COSI, DH, IS, LACSEA, LS&C, MATH, pcAOP)*. Optical Society of America, 2018, p. CTH1B.1. [Online]. Available: <http://www.osapublishing.org/abstract.cfm?URI=COSI-2018-CTH1B.1>
- [45] A. J. D'Alfonso, A. J. Morgan, A. V. Martin, H. M. Quiney, and L. J. Allen, "Fast deterministic approach to exit-wave reconstruction," *Phys. Rev. A*, vol. 85, no. 1, p. 13816, jan 2012. [Online]. Available: <https://link.aps.org/doi/10.1103/PhysRevA.85.013816>
- [46] I. S. Wahyutama, G. K. Tadesse, A. T  nnermann, J. Limpert, and J. Rothhardt, "Influence of detector noise in holographic imaging with limited photon flux," *Opt. Express*, vol. 24, no. 19, pp. 22 013–22 027, sep 2016. [Online]. Available: <http://www.opticsexpress.org/abstract.cfm?URI=oe-24-19-22013>
- [47] A. V. Oppenheim and R. W. Schaffer, *Discrete-Time Signal Processing*, 3rd ed. Upper Saddle River, NJ, USA: Prentice Hall Press, 2009.

- [48] E. Candès, Y. Eldar, T. Strohmer, and V. Voroninski, "Phase Retrieval via Matrix Completion," *SIAM Review*, vol. 57, no. 2, pp. 225–251, 2015. [Online]. Available: <https://doi.org/10.1137/151005099>
- [49] The Center for X-ray Optics, Lawrence Berkeley National Laboratory. (2010) X-ray transmission of solids. [Online]. Available: http://http://henke.lbl.gov/optical_constants/filter2.html
- [50] W. Trench. (N.D.) Inverses of lower triangular toeplitz matrices. Unpublished. [Online]. Available: http://ramanujan.math.trinity.edu/wtrench/research/papers/TRENCH_TN_6.PDF
- [51] G. Strang, *Introduction to Linear Algebra, Fifth Edition*. Wellesley-Cambridge Press, 2016. [Online]. Available: <https://www.amazon.com/Introduction-Linear-Algebra-Gilbert-Strang/dp/0980232775?SubscriptionId=AKIAIOBINVZYXZQZ2U3A{&}tag=chimbori05-20{&}linkCode=xm2{&}camp=2025{&}creative=165953{&}creativeASIN=0980232775>
- [52] W. Schottky, "Über spontane Stromschwankungen in verschiedenen Elektrizitätsleitern," *Annalen der Physik*, vol. 362, no. 23, pp. 541–567, 1918. [Online]. Available: <https://onlinelibrary.wiley.com/doi/abs/10.1002/andp.19183622304>
- [53] K. He, M. K. Sharma, and O. Cossairt, "High dynamic range coherent imaging using compressed sensing," *Opt. Express*, vol. 23, no. 24, pp. 30 904–30 916, nov 2015. [Online]. Available: <http://www.opticsexpress.org/abstract.cfm?URI=oe-23-24-30904>